Verifying of ‘Orifice Plate’ connecting duct lengths to validate the performance of a ‘Vent Test Rig at Australian Maritime College’ by Computational Fluid Dynamics (CFD) as part of the Oscillation Water Column Power Take-Off

MCP Dissanayake
Department of Marine Engineering, Faculty of Engineering, General Sir John Kotelawala Defence University, Sri Lanka
[#] dissanayakemcp@kdu.ac.lk

Abstract— *Oscillating Water Column (OWC), ocean wave energy converter that transforms energy of ocean wave into low-pressure pneumatic power. This pneumatic power is extracted by a turbine and converting to electric energy through a generator. Australian Maritime College (AMC) was set up a vent test rig to conduct experiments on 'OWC' operation, quantify the air leakage and find differential pressures across the orifice plate as per Australian standard of fan performances. However, the upstream and downstream duct lengths of the vent test rig were not matched with given specified standards due to space restriction. Therefore, the technical team of AMC was chosen Computational Fluid Dynamic (CFD) application as an alternative method to continue the investigation with the economy of effort. Subsequently, it is understood that CFD is a very attractive method to carry out the investigation and able to obtain a detailed report with all tested parameters and conditions. In addition, it is revealed that the shape of the flow pattern, which cannot see during the experimental study. The objective of this investigation was to apply CFD instead of vent test rig experiment and carry out modeling, then compare outcomes with experimental results. Further, CFD application was used to test differential pressure across the orifice plate with the same upstream and downstream lengths of pipe, that utilized during the vent test rig experiment. In addition, CFD has been applied again for specified lengths of pipe with the same orifice plate to measure the differential pressure across it. Finally, it was proven that specified duct lengths were directly impacting to performance of the vent test rig and decreasing the generating pressure along with the length of the pipe due to relative roughness.*

Keywords— Oscillating Water Column, Inflow Radial Turbine, Vent Test Rig, Orifice Plate, Computational Fluid Dynamic.

I. INTRODUCTION

Oscillating Water Column (OWC), an ocean wave energy converter that transforms the energy of ocean waves into low-pressure pneumatic power. This pneumatic power is extracted by a turbine and converting to electric energy through a generator. Australian Maritime College (AMC) was set up a vent test rig to conduct experiments on 'OWC' operation, quantify the air leakage and find differential pressures across the orifice plate as per Australian standard of fan performances. However, the upstream and downstream duct lengths of the vent test rig were not matched with given specified standards due to space restriction. Therefore, the technical team of AMC was chosen Computational Fluid Dynamic (CFD) application as an alternative method to continue the investigation with the economy of effort.

Computational Fluid Dynamic (CFD) simulation is cost-effective, quick outcome and attractive in nature compare to experimental investigations. Further, it is providing a detailed report with all tested parameters and conditions. Moreover, it is revealed that the shape of the flow pattern, which cannot see during the experimental study. Generally, CFD permits for the modeling of extra complications, that affect the outcomes. When flow pattern is showing, high-fidelity CFD simulations will make available detailed statistics in the calculation domain. Add advantages of this CFD simulation are to repeat the same conditions and situations and obtain accurate results. Making pipe geometry was not much complexity in this CFD simulation. ANSYS was applied and used lots of energy to obtain superior pre-processing and established high fidelity turbulence models, such as the Large Eddy Simulation model and Reynolds average Naiver-Stokes model. Then, CFD was applied to resolve the turbulent problem utilizing a super-grid scale and could practice empirical models for sub-grid turbulent structures (Leap CFD team, 2015).

The objective of this investigation was to apply CFD instead of vent test rig experiment and carry out modeling, then compare outcomes with experimental results. Further, CFD application was used to test differential pressure across the orifice plate with the same upstream and downstream lengths of pipe, that utilized during the vent test rig experiment. In addition, CFD has been applied again for specified lengths of pipe with the same orifice plate to measure the differential pressure across it.

Figure 1: Vent Test Rig to Test OWC Operation (Australian Maritime College).

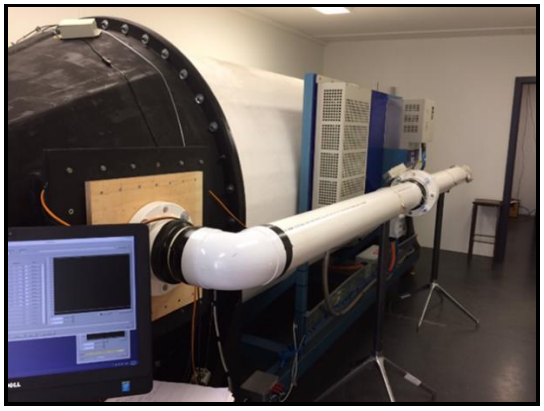

II. DESIGN FEATURES

In this simulation, the differential pressures, mass flow rate, and piston velocities were investigating by CFD application based on the following equation (1). The vital factors of this experiment were to maintain adiabatic condition, the effectiveness of sealing, a consistent control arrangement, coaxially fixing the orifice, installing exact duct lengths, the precise placing of pressure sensors, temperature sensors, and smooth mechanical operations to obtain accurate consequences.

$$C = \frac{q_m\sqrt{1-\beta^4}}{\frac{\pi}{4}d^2\sqrt{\Delta p \rho_1}} \quad (1)$$

$$\beta = d / D \quad (2)$$

Where, β is Diameter Ratio

d is Diameter of Orifice

D is Diameter of Duct

Reynold Number Effects

Exploiting the correct flow pattern was vital in the vent test rig operation to acquire the correct measurement of airflow. Reynold's number-based equation (2) was utilized to calculate the measurement. Required Reynold number was fluctuating as per variation of the parameters, of the equation. Though, vital to encompasses the practically viable and lucrative method to change the parameters during the experiment.

The changing kinematic viscosity (ν) was effortless, though, altering other parameters was to developed more pressure inside the vent test rig. The variation of the test facility and compressibility effects were deliberated restrictive influences to transform the kinematic viscosity during the test. The generated velocity was maintained between 0.06 m\s to 0.31 m\s to accomplish the Reynold number. The industrial fans- performance testing standards was emphasizing that the Reynold number might be ignored. Though, confirm to continue the Reynold number was keeping more than 3 x 10^6. Further, the diameter of the prototype needs to be at least 0.9 m or model scale 1/5th, whichever should be larger.

$$Re = \frac{\rho v l}{\mu} \quad (2)$$

Velocities (m\s)	Re of Upstream (1675 mm)
0.06	6.81 x 10^3
0.1	1.12 x 10^4
0.11	1.21 x 10^4
0.14	1.61 x 10^4
0.15	1.73 x 10^4
0.24	2.71 x 10^4
0.25	2.82 x 10^4
0.3	3.41 x 10^4
0.31	3.5 1 x 10^4

Table 1: Fluctuations of Reynold number as per different pipe lengths

Coefficients of Orifice Plates

Many types of standard orifice plates can be utilized for the experiments, though all of them need to be alike, with only one explanation. More, all type of standard orifice plates is to be distinct as per positioning of pressure tapings. The detailed schematic of the standard orifice plate is shown in figure 2. The standard orifice plate is comprising of a thin circular plate of two flat faces with a 90 mm diameter of an orifice. Moreover, the orifice was positioned coaxially to the pipe center with a straight line and uphold the thickness of the plate between 0.005D to 0.02D. Usually, more attention was paid to the fabrication process of the orifice plate and ensure the sustainability of the developing pressures and avoid plastic buckling and deformation taking place during the experiment.

$$Re = \frac{\rho v l}{\mu} \quad (11)$$

Figure 2: Schematic of Orifice Plate Application

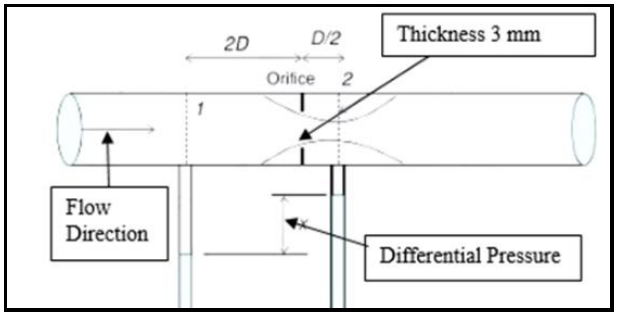

The vent test rig was operated in different velocities in steady-state conditions and selected three velocities were to make an easy comparison with CFD outcome. The flowrate and differential pressures across the orifice plate were obtained through the control system and tabulated in table 2.

Table 2: Experimental Results

Velocity (m/s)	Generated Air Flow by the Piston (m^3/s)	Inlet Pipe Pressure at Short Pipe (Pa)	Outlet Pipe Pressure at Short Pipe (Pa)
0.06	0.118	197	113
0.15	0.132	1258	923
0.25	0.54	3490	2052

Figure 3: Inlet pressure variation upstream of a pipe

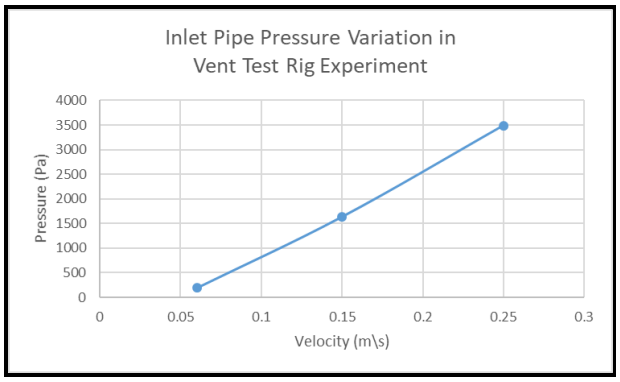

Figure 4: Outlet pressure variation downstream of a pipe

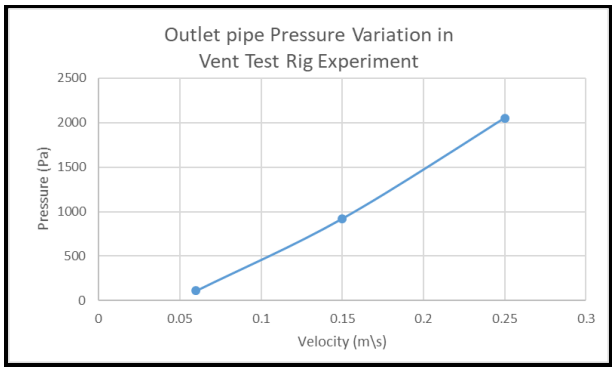

Vent Test Rigs' Operation

A servo motor operated vent test rig was comprised of 3000 mm in length and piston diameter of 1500 mm chamber, and generate the basic airflow features of an OWC, ocean energy extraction. The vent test rig was right scaled and set up with a volume of 3.534 m^3. Further, the vent test rig was operated in the range of velocity from 0 to 1.25 m/s. All the measurements were carried out in the adiabatic condition at ideal gas air velocity not as much as 1.25 m/s, chamber pressure, below 5 kPa, and dry air density in 1.225 kg/m^3. The block orifice plate was fixed between upstream and downstream of the pipe to assess the leakage of air and related uncertainty occurring inside the vent test rig. A 'PVC' is chosen as a suitable material for the duct with a 150 mm diameter to fulfill the ISO 5167, standards. A specified range of diameter of the duct was not less than 50 mm and not more than 1200 mm, either application of Reynold number should be more than 3150. Installed pressure sensors and temperature sensors were factory calibrated and fixed through the drilled holes of the upstream and the downstream of the duct adjacent to the orifice plate to obtain the outcome. The upstream and downstream pipe lengths were taken as 1675 mm and 1800 mm respectively, due to the limited space in the room. The orifice diameter was 90 mm and established pressure wall with a distance of 150 mm from the orifice plate to the upstream and 75 mm to the downstream. The static pressure and differential pressure (Δp) were measured through pressure sensors. According to fan performance standards, the stated diameter ratio (β) of the orifice was selected through the given charts and fabricated the orifice plate. Subsequently, it is placed between upstream and downstream of the duct coaxially with a straight line to maintain the uniform flow of air.

Developing a Geometry

The 3-D geometry of two pipes and orifice was generated by Inventor software and exported to ANSYS 19.1 workbench software shown in figures 4 & 5.Subsequently, a fixed diameter orifice was made and selected x, y, and z coordinates correctly, then developed upstream duct length with 1.675 m and downstream duct length with 1.8 m as a condition one. Then simplify the geometry by introducing inlet, outlet, walls, orifice inlet, and orifice outlet to the ducts and orifice. Similarly, the upstream duct length was extended up to 3 m and the downstream duct length was shortened to 1.2 m, as per given standards with the same orifice as a condition two.

Figure 5: Geometry of the Short Pipe

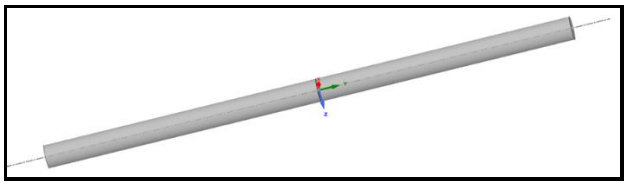

Figure 6: Geometry of the Long Pipe

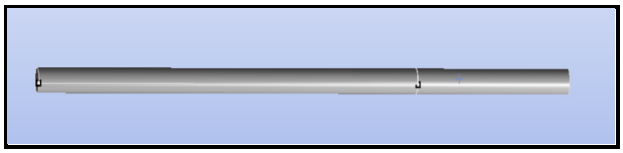

Generate a Mesh

The mesh generation is a pre-processing phase of the computational fluid dynamic simulation and the discretization of the domain. The process of meshing is a time-consuming and complex affair to generate an accurate mesh. The mesh is essential to be in quality to give accurate answers. The movement of flow is a bit complex in this application and approach with the coarse mesh to begin the task. The meshing process is comprised of two categories such as structured and unstructured meshes. A numbering of structured mesh cells or nodes are described as (i, j, k) indices at the Cartesian coordinate structure with interior nodes and surrounded by the constant number of elements Moreover, unstructured mesh cells are specified with a point to point connections between nodes and significantly affect the modeling software. The hybrid mesh is consisted of a combination of structured and unstructured meshes and

providing additional provisions during the meshing. The significant controlling effect of the nods and sufficient to operate fewer memory capacities of the computers for structured meshing in process of referencing of cells. This application can be handled by even unskilled operators during the meshing process and the possibility to obtain better results with fewer nodes (Seo, J.H., Seol, D.M., Lee, J.H. and Rhee, S.H., 2010).

The mesh was generated using ANSYS Meshing 19.1, with physics and solver preferences set to CFD and CFX respectively. The constraint was imposed up to 512,000 nodes and completed the fine mesh, as per table 2 and shown in figures 6 & 7.

Figure 7: Fine Mesh of Short Pipe, Inlet Face

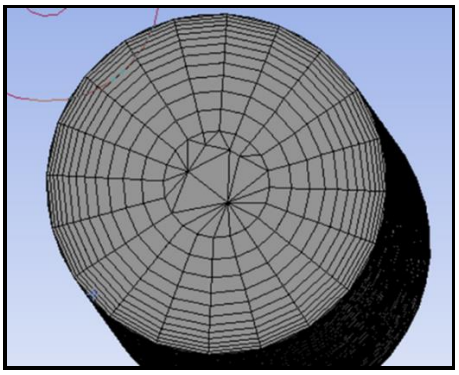

Figure 8: Application of Fine Mesh of Short Pipe

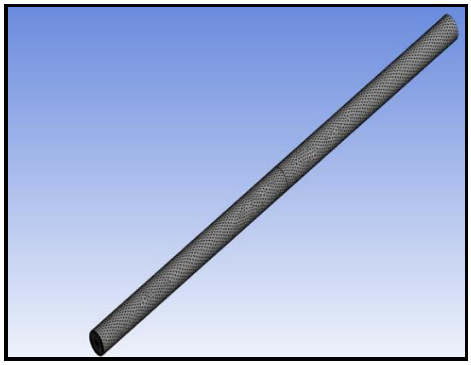

Figure 9: Application of Fine Mesh of Long Pipe, Inlet Face

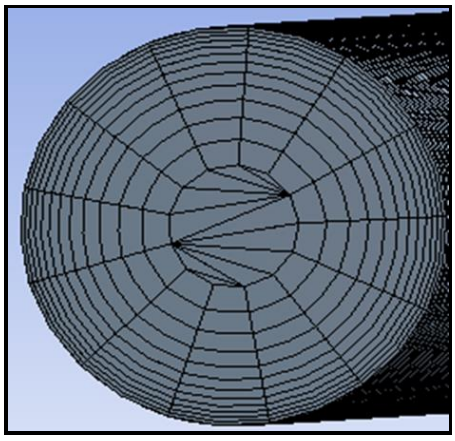

Figure 10: Application of Fine Mesh of Long Pipe

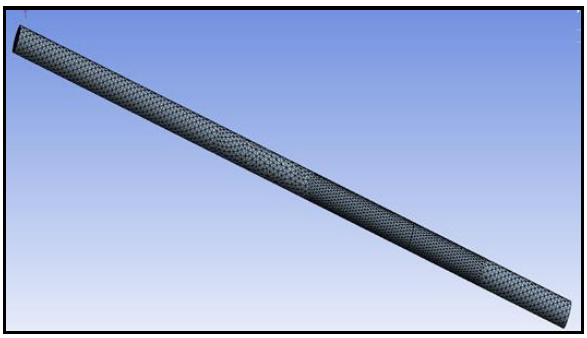

Calculation of Inflation Layer

The inflation layer was established based on boundary layer modeling theory and ensure to develop the inflation layer thickness fully exceeded the boundary layer thickness. The calculation was carried out as per the following equation at (3).

$$Y_{BL} = 0.16.\ x/\ (Re_x)^{1/7} \qquad (3)$$

Where, x is critical length

Y_{BL} is turbulance boundary layer height

The boundary layer was modeled by low Reynold number wall treatment consisted of a y+ value of 1 and a growth rate of 120% laminar sublayer that made the pathway capture the outcome of frictional resistance and separation.

Table 3: Application of Low Reynold Treatment and Wall Function.

	Low Reynold wall treatment	Wall function
	y+1	y+30
L[m] (chord length)	1	1
Viscosity	1.512×10^{-5}	1.512×10^{-5}
Density	1.225	1.225
Speed [m/s]	0.25 m\s	1
Re	1,000,000	1,000,000
Y BL [m]	0.04446	0.04
y+	1	30
Delta Y 1st layer	0.00	0.000719843
Growth rate	1.2	1.2
Tol. Inflation (maximum thickness in analysis)	0.049091633	0.051853955
No. Layers		27

CFX Pre Solver

The mesh files were imported into CFX Pre Solver and conducted the analytical study. Then defined the properties of air and boundary conditions. The two numbers of monitoring points were established with 0.15 m distance from the orifice plate inside the upstream of the pipe as per specified standards. Similarly, two more numbers of monitoring points were set up with 0.075 m distance from the orifice plate inside the downstream of the pipe to obtain relevant measurements of the pressures. The mass flow rate was calculated as per piston moving velocity and fed as an input to the application and obtain the related pressure by monitor points.

Table 4: Details of Input Mass Flowrate to CFD application

Velocity (m\s)	Input Mass Flowrate (kg\s)
0.25	0.54
0.15	0.32
0.06	0.129

Analysis Procedure

An analytical setup was recognized in a steady state to avoid all time and computational source restrains. The face sizing was conducted to diminish errors and maximize separation areas. The turbulence model is selected as per the resolution and place of nodes inside the boundary layer. According to the proper selection, low Reynold wall treatment is being applied with y+ = 1, and the Shear Stress Transport (SST) turbulence model is being chosen to model-free stream and boundary layer turbulence.

Boundary Condition

The boundary conditions were applied in ANSIS 19.1 pre and boundary regions have been decided to solve the problem in the best way. The inlet flow of the duct, pressure monitor points of either side of the orifice plate, and outlet of the duct are shown in figure 5. The inlet and outlet domains were modeled and with air in three different velocities shown in table 4. The inlet and outlet pressures were monitored through monitoring points and carry out the simulation, then it ensures to get convergence in inlet pressure variations along with velocities.

Table 5: Application of Boundary Conditions

	Type of Boundary	**Situations**
Pipe Inlet	Inlet	Velocity is varying from 0.06 m\s, 0.15 m\s and 0.25 m\s.
Pipe Outlet	Outlet	
Wall	Wall	

Figure 11: Boundary condition details of Short pipe

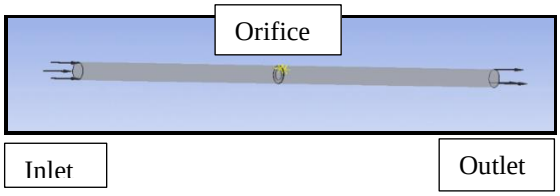

Figure 12: Boundary condition details of Long pipe

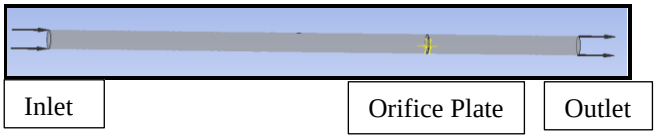

Solution Control

The solution control application was used to defined solver control inputs and convergence criteria, then set up the system to make use of the resources efficiently at table 4.

Table 6: Control Inputs

Solver Control Inputs	
Maximum Iterations	500
Maximum Iterations	5000
Criteria for the Convergence	
Type of Residual	RMS
Residual of the Target	0.0000001

CFX Solver Application

The CFX solver files were written for the different pressures all as per velocities in two different pipe lengths in separate computers using 7 cores. The studied variables and examined the convergence explanations, before exporting the solution files.

Verifications

A grid independence study was conducted to examine mesh reliability on different pressures across the fixed diameter orifice, during two different lengths of pipes. A Richardson Extrapolation was conducted to authenticate the three sets of mesh resolutions and specified them as 'coarse', 'medium', and 'fine'. In addition, all three mesh types were ruled by modification of, face sizing with support of inflation layers. The Richardson extrapolation method was applying to impact the mesh size and anticipate the constant expansion ratio for node count of the mesh. The Richardson Extrapolation prediction was based on the expansion ratio along with the non-dimensional coefficients and emphasized that the solution of a mesh sufficed with infinite nodes. Subsequently, results of the coarse, medium and fine meshes were assessed in line with a comparative error related to the Richardson-extrapolate clarification. The calculation of Richardson Extrapolation is cited in Appendix B.

Sensitivity Study of Mesh

A mesh sensitivity research was conducted to confirm the optimization of meshing to solve the problem and ensured the obtained outcome which was totally independent of the quality of the mesh. The mesh refinement was done by changing face sizing and kept other parameters constant. All three types of meshes are specified in table 6. The mass flow rate was fed as per input to the inlet of the duct.

Subsequently, pressures of specified two number of monitor points were provided the measurement of pressures that located either side of the orifice plate of the pipe and indicated by the cartesian coordinates.

Convergence Study for Short Length Pipe

The inlet pressure is converged with an estimated error of 0.0352, 0.021, and 0.0175 for the coarse, medium, and fine mesh respectively, at the velocity of 0.25 m\s for the short-length pipe. It was revealed that the fine mesh providing the minimum error compare to other meshes. Thus, the fine mesh was designated to conduct the analysis process. The plot is clearly specified that the highest inlet pressure at fine mesh, then second-highest inlet pressure at the medium mesh, and finally lowest inlet pressure at the coarse mesh in figure 9. Further, it is meeting the requirement of grid convergence theory. The details of the convergence study for short-length pipe are shown in table 7.

Table 7: Number of Nodes and Sizes of Short Pipe

Type of Mesh	Number of Nodes	Number of Elements	Size	Inflation Thickness
Coarse	23904	50703	0.0352	0.1
Medium	73223	152726	0.021	0.1
Fine	113093	236585	0.0175	0.1

Figure 13: Application of Grid Convergence to the Short pipe

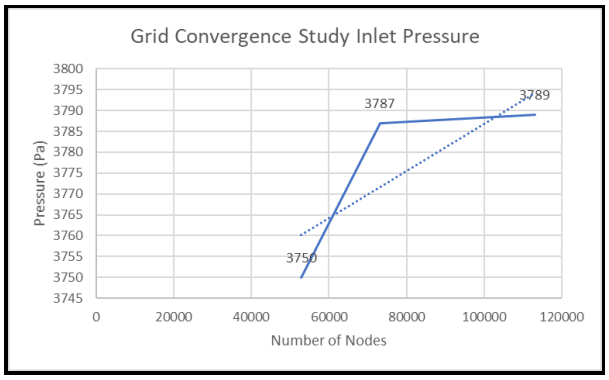

Convergence Study for Long Length Pipe

The inlet pressure is converged with an estimated error of 0.04, 0.0395, and 0.039 for the coarse, medium, and fine mesh respectively, at the velocity of 0.25 m\s for a long length pipe. It was revealed that the fine mesh providing the minimum error compare to other meshes. Thus, the fine mesh was designated to conduct the analysis process. The plot is clearly specified that the highest inlet pressure at fine mesh, then second-highest inlet pressure at the medium mesh, and finally lowest inlet pressure at the coarse mesh in figure 10. Further, it is meeting the requirement of grid convergence theory. The details of the convergence study for short-length pipe are shown in table 9.

Table 8: Number of Nodes and Sizes of Long Pipe

Type of Mesh	Number of Nodes	Number of Elements	Size	Inflation Thickness
Coarse	229961	95054	0.04	0.1
Medium	232451	96318	0.0395	0.1
Fine	263527	236585	0.039	0.1

Figure 14: Application of Grid Convergence to the Long pipe

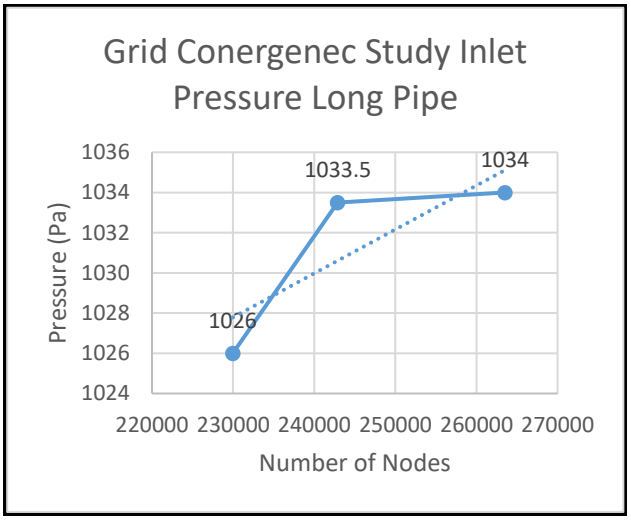

Table 9: Details of Convergence Study for Long Pipe

Mesh	Size	Nodes	Elements	Inlet CFD (Pa)
Coarse	0.04	229961	95054	1021
Medium	0.0395	242876	96318	1025
Fine	0.0175	263527	236585	1030

III RESULTS AND DISCUSSION

Short Pipe

According to three different piston velocities of the vent test rig, the mass flow rate was calculated and fed as input to the inlet of the boundary condition one. Subsequently, the pressures were obtained through the monitoring points that were established across either side of the orifice plate in line with specified standards shown in table 7. Both inlet pressures of experimental results and CFD outcomes were increasing with the advancement of velocities. The percentage difference is (-2.53) at 0.06 m\s, (-1.77) at 0.15 m\s and (-0.57) at 0.25 m\s during the comparison and shown in figure 14. Similarly, outlet pressures were growing along with the advancement of velocities. However, the percentage difference is (-3.53) at 0.06 m\s, (-0.68) at 0.15 m\s, and (-1.07) at 0.25 m\s during the comparison and bit vary from the inlet pressure difference, due to orifice plate effect and shown in figure 15.

Table 10: Comparison of Pressures, Short Pipe

Velocity	P1 (Inlet)	P2(Outlet)	

(m\s)	CFD (Pa)	EFD (Pa)	%	CFD (pa)	EFD (pa)	%
0.06	192	197	-2.53	109	113	-3.53
0.15	1250	1258	-1.77	724	729	-0.68
0.25	3470	3490	-0.57	2030	2052	-1.07

Figure 15: Assessment of Experimental Outcome and CFD Outcomes of Inlet Pipe

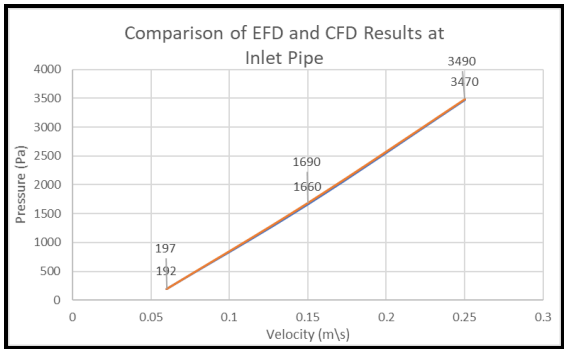

Figure 16: Assessment of Experimental Outcome and CFD Outcomes of Outlet Pipe

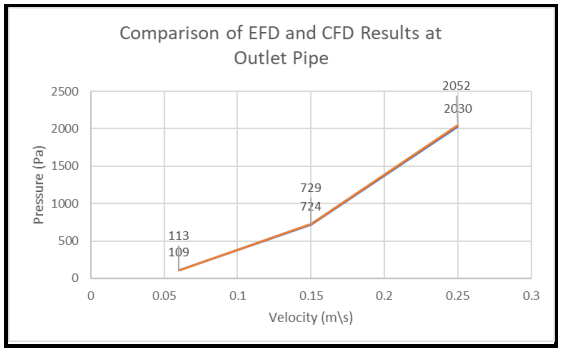

Figure 17: Results of Velocity 0.25 m\s, short pipe.

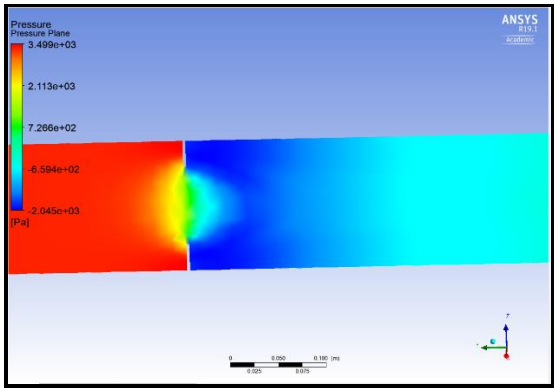

Figure 18: Results of Velocity 0.15 m\s, short pipe.

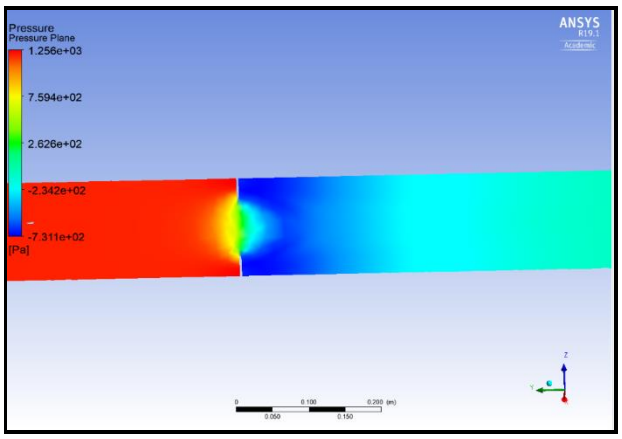

Figure 19: Results of Velocity 0.06 m\s, short pipe.

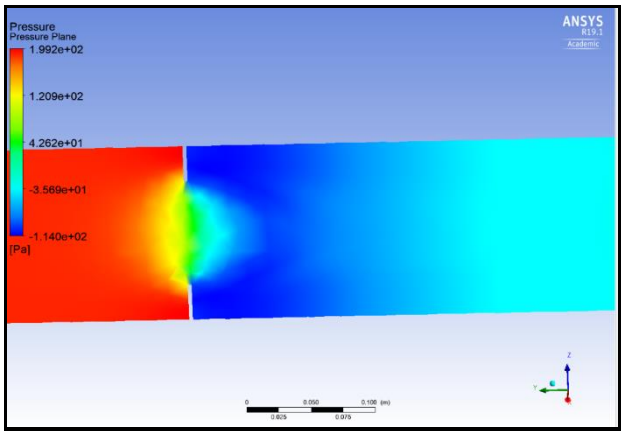

Long Pipe

There were no experimental results in the process and only CFD results were obtained through monitoring points. On this occasion, the inlet pipe was 3 m and the outlet pipe was 1.2 m, the input variables were applied similar to condition one and obtained the pressures from the monitoring points, and shown in table 7. Compare to short pipe, both inlet pressure and outlet pressures were low in the long pipe due to the effect of relative roughness shown in Figures 20 & 21.

Table 12: Comparison of Pressures, Long Pipe

Velocity (m\s)	Inlet	Outlet
	CFD (Pa)	CFD (Pa)
0.06	1021	12.9
0.15	1025	32.8
0.25	1030	54

Figure 20: Results of Inlet of Long Pipe

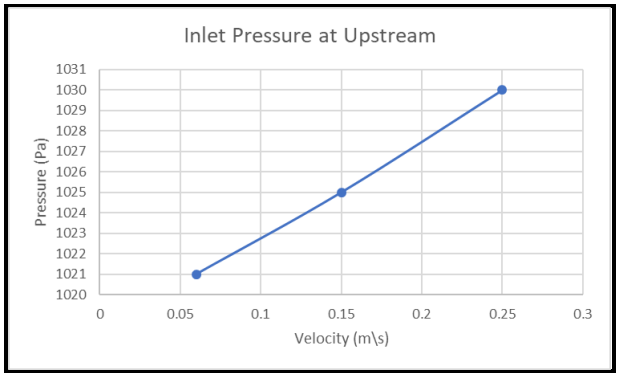

Figure 21: Results of Outlet of Long Pipe

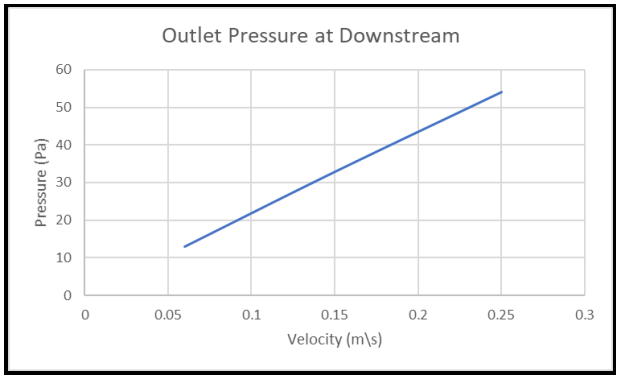

Figure 22: Results of Velocity 0.25 m\s, long pipe

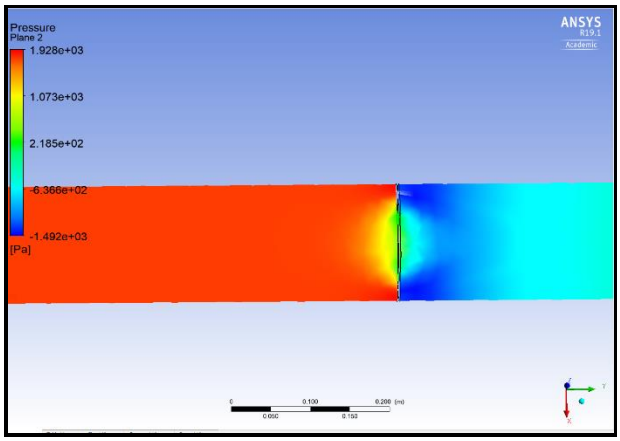

Figure 23: Results of Velocity 0.15 m\s. long pipe

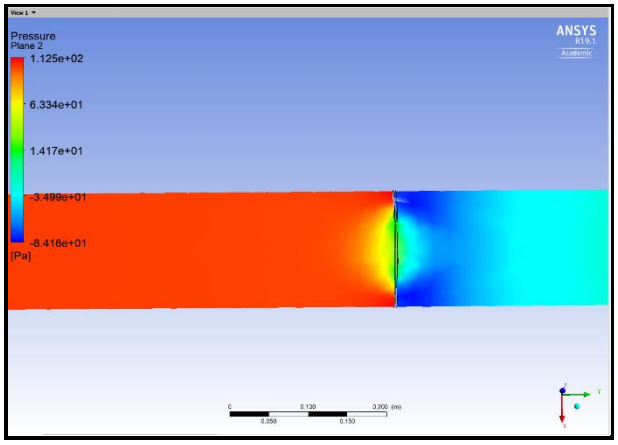

Figure 24: Results of Velocity 0.06 m\s, long pipe

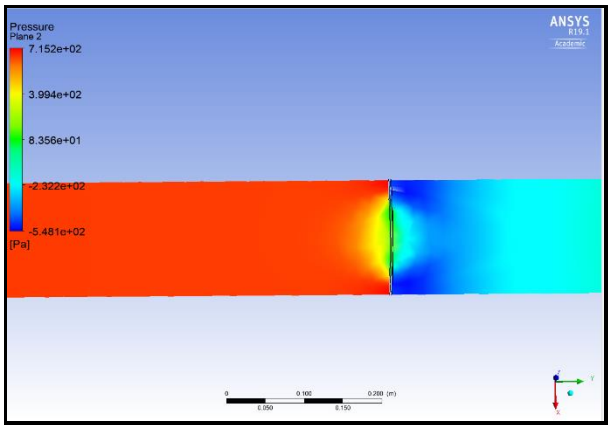

According to figures 16, 17, 18 related to the short pipe and figures 21, 22, 23, of the long pipe, it is revealed that the pressure development through the orifice plate was high when the upstream pipe was the short and uniform flow of outcome was showing due to sufficient length of downstream of pipe. When the upstream of the pipe was lengthy, the pressure generated through the orifice plate was reduced due to relative roughness, and outlet pressure further, dropped down. The total pressure is encompassed with radial variations and circumferential variations. Radial variations are generated causing boundary layers' effect and influence for the result. Though, circumferential variations are developed due to the tangential element and insignificant.

IV. CONCLUSION

The CFD application was proven that specified duct lengths were directly impacting to performance of the vent test rig and decreasing the generating pressure along with the length of the pipe due to relative roughness.

REFERENCES

Fleming, A., MacFarlane, G., Hunter, S., and Dennis, T., 2017. Power performance prediction for a vented oscillating water column wave energy converter with a unidirectional air turbine power take-off. In Proceedings of the 12th European Wave and Tidal Energy Conference (pp. 1204-1). EWTEC.

Fleming, A.N., 2012. Phase-averaged analysis of an oscillating water column waves energy converter (Doctoral dissertation, University of Tasmania).

Herring, S., 2007. Design and evaluation of turbines for use in OWC power plants.

AMC Lecture Notes.

Bauman, R.P. and Schwaneberg, R., 1994. Interpretation of Bernoulli's equation. The Physics Teacher, 32(8), pp.478-488.

LEAP CFD Team, 2013. How does the Reynolds Number affect my CFD model? URL: http://www. computational

fluid dynamics. com. au/Reynolds-number-CFD/ [cited May 2015].

CFD Online, 2012

ABBREVIATIONS AND SPECIFIC SYMBOLS

ACKNOWLEDGMENT

I would like to acknowledge my supervisor Dr. Alan Fleming (Australian Maritime College) for his guidance kind assistance and cordial relationship throughout this research project. I would like to thank Mr. Liam Honeychurch for his support to set up the vent test rig. Finally, I would like to thank Mr. Michael Underhill for his contribution to establishing the orifice plate and related duct installation.

AUTHOR BIOGRAPHIES

Cmde (E) MCP Dissanayake, CEng (India) is currently performing as the Head of Department (Marine Engineering) and holds 2 No's patents for his research papers published so far. He is an inventor and published 06 No's publications on Brackish Water Reverse Osmosis application, Fan Boat Building and Oscillation Water Column, Ocean Wave Energy Converter. He was the Director in Research & Development at Sri Lanka Navy and has received commendations on a number of occasions from the Commander of the Navy, HE the President of Sri Lanka for his innovation. Further, he was awarded the prestigious, Japanese, Sri Lanka Technical Award for his own developed low-cost Reverse Osmosis Plant, to eliminate Chronic Kidney Disease from Sri Lanka. Moreover, he has vast exposure to marine diesel engines and possesses a Masters's degree in Marine Engineering from Australian Maritime College, University of Tasmania, Australia.